Experimental Results
Experimental Monitoring of Nonlinear Wave Interactions Under Uniaxial Load

Alison E. Malcolm, Lauren Coates, Kamal Moravej, Andrey Melnikov, Steve Butt, Kristin M. Poduska

Supporting Information

This supporting information gives additional detail on the experimental setup not necessary for understanding the results, but necessary for duplicating the experiments. In addition, we discuss the modeling of the strain induced by the pump and the cumulative strain observed by the probe.

S.1 Measuring Velocity at Different Loads

It is important to calibrate transducers to have accurate travel time measurements by measuring the travel time through different thicknesses of the same material and finding the intercept time. This intercept time measures the inherent delay from the transducer. For our transducers this number is 0.3 μs for S and 0.5 μs for P; we apply these corrections to the measured travel times before computing the associated velocities. To measure the velocities shown in Table Table 2and Figure Figure 2, we first pick the travel times. For the lowest applied load (1 MPa), this is done by picking the zero-crossing before the peak within a user-defined time window. Each pick is then manually checked to ensure that it chose the correct arrival. For higher loads, we measure the travel time change by cross-correlating the waveforms with those recorded at 1 MPa. When we extract the P-wave velocity from measurements of the S-wave PUMP, we are using what are sometimes referred to as parasitic P-waves, generated by S-wave transducers. In this case, the P-wave is much smaller than the S-wave and so to recover a reliable velocity change we window the data to include only the P-wave. This methodology along with estimates of the errors in P-wave velocities inferred from such parasitic waves is described by Yurikov et. al. Yurikov et al. (2019); they report errors of 5% compared with traditional methods of measuring P-wave velocities with P-wave transducers. We do not need to window when measuring the S-wave travel time because the S-wave is much stronger. For measurements on the probe signals, we record only about 2 periods of the signal and so there is no interference between different wavetypes. We measure the dimensions of the samples with calipers and use them to convert the travel times to velocities; these values are given in Table Table 2. We use the repeated measurements on the PUMP signals (for the two probes) to estimate the errors in our recovered velocities at less than 5%, in line with the errors observed by others Yurikov et al. (2019) from using parasitic P-waves from S-transducers.

S.2 Experimental details

All signals are generated with a standard (Agilent 33500B Series) function generator and recorded with a standard (KEYSIGHT InfiniiVision MSOX2014A) 8-bit oscilloscope. The PUMP signals are amplified with an (E & I 240L RF) power amplifier and all recorded signals are high-pass filtered with a (Krohn-Hite) adjustable digital filter with cut-off frequency of 600 kHz. Each recorded signal is an average of 4096 signals to reduce noise and sampled every 4 ns; example signals are shown in Figure S.1. The signals are recorded at the lowest vertical range on the oscilloscope that does not result in clipping the recorded signal, this maximizes the accuracy of the recorded probe signal. This ranges from 1-200 mVp-p, except for when we record the PUMP alone (dotted lines in Figure Figure 1) where the scale is 150 Vp-p.

We use Olympus transducers, specifically V-153 (S, 1 MHz, 1.3 cm diameter), V-103 (P, 1 MHz, 1.3 cm diameter) for the two probes and the V-1548 (S, 100 kHz, 2.5 cm diameter) for the PUMP. The driving frequencies of all transducers are chosen to give a signal recorded on the opposite face that most closely resembles our ideal waveform. For the pump this is a four-cycle sinusoid, and for the probe this is a one-cycle sinusoid. Example signals are shown in Figure S.1.
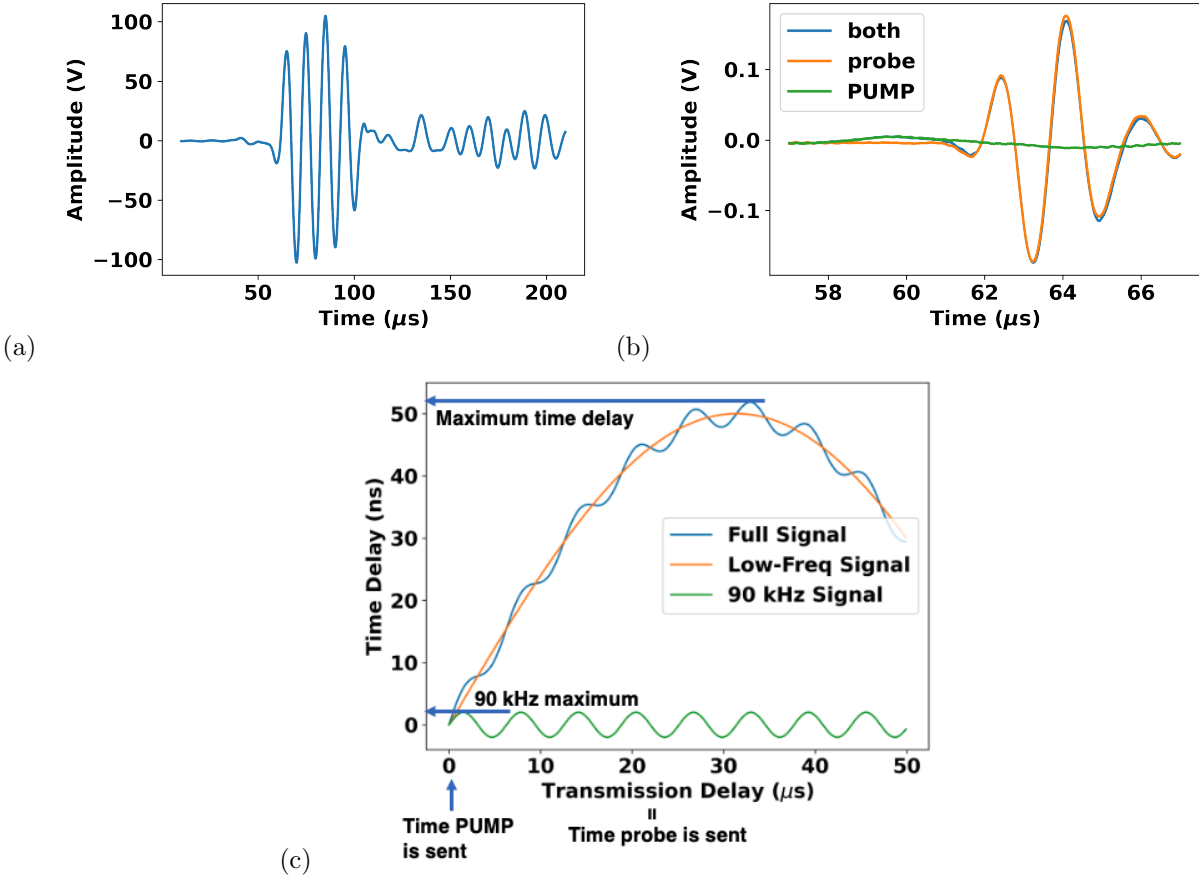
Figure S.1: (a) PUMP signal recorded on the x-face of the sample opposite the PUMP generating S-wave transducer. (This signal uses the recording setup with the dashed lines in Figure Figure 1.) (b) Signals recorded to estimate travel time delays on the P-transducer on the y-face opposite the P-probe source transducer. (These signals use the recording setup shown with the solid lines in Figure Figure 1.) The three signals shown are with the PUMP only (S_2), the probe only (S_1) and both together, (S_3). These signals have been filtered to remove as much of the PUMP signal as possible. Note the different scales in both time and amplitude. (c) Cartoon to illustrate the format of the data plots (shown in Figure Figure 3).

All of our experiments were performed at room conditions, in an interior climate-controlled room. We wrapped the sample in plastic wrap to diminish the influence of humidity changes on the results. We would certainly expect to see changes in that environment over the course of the experiments, and the local humidity over the period of the experiment averaged 83% with significant excursions to a high of 100% and low of approximately 40%, with all days averaging between 75 and 95% and no consistent trends. Experiments were completed on each sample and probe before moving to the next to minimize the effect of variations in room conditions on the results. Khajehpour Tadavani et. al. Khajehpour Tadavani et al. (2020) find that humidity changes impact the results, but that these impacts have an exponential time constant on the order of days to weeks for these samples, in other words these changes happen slowly compared to our experimental time.

S.3 Measuring the strain

This strain is measured using a laser-doppler vibrometer and averaging the amplitude (measured from the peak of the Hilbert transform of the signal) of the recorded particle velocity signals at several locations on the sample. We then divide the recorded particle velocity by the phase velocity of the recorded wave. This gives an estimate of the strain assuming that we are exciting plane waves. Because this assumption is not strictly true, we are confident only that this gives us the order-of-magnitude of the strain and that it gives us a good measure of the relative magnitude of the two strains. This protocal has been used before Gallot et al. (2015), but we repeat it on this sample in our laboratoryKhajehpour Tadavani et al. (2020).

S.4 Computing the travel time delays

We compute the travel time delays plotted on the y-axis in Figure Figure 3by fitting a sinc function to the five points nearest the peak of the cross-correlation of the two signals. This follows the suggestion of e.g. Catheline et al. Catheline et al. (1999), replacing the parabola with a sinc function because in fitting the peak we are essentially assuming that we have undersampled our signals, for which a sinc interpolation is the optimal solution (Ali Gholami, personal communication, 2018). Our numerical experiments using one-cycle sine waveforms shifted by a known amount indicate that we can estimate a travel time delay with two digits of accuracy down to approximately 1/100 of our sampling interval (i.e. the error in our travel time estimate is 0.04 ns).

S.5 Modeling the PUMP strain

We are interested in traveling waves because, in the field, transient signals are easier to excite than resonance modes. To achieve this in our experiments, we send only four cycles of the PUMP, and at a frequency such that this PUMP does not excite the entire sample simultaneously. As a result, our probes sense a much more complicated strain than what occurs in resonance-based DAET Renaud et al. (2008). To explore this further, we present a simple numerical model of the experiment, based on a finite-difference implementation of the elastic wave equation Virieux (1986); Graves (1996) to determine what the probe senses as it travels across the sample.

Our model estimates the cumulative strain, caused by the PUMP, that is sensed by the probe wave during our experiments. We simulate PUMP propagation and estimate the resulting strain distribution as a function of position in the sample and propagation time. Examples of strain field snapshots are shown in Figure S.2.

We use calculated strains to compute the cumulative strain experienced by the probe as it travels across the sample, perpendicular to the PUMP propagation direction. In our experiments, we analyze only the arrival time of the probe, so we expect that the strain experienced by the first part of the probe waveform is most important. As a result, it is not necessary to model the probe propagation. Instead, we compute (analytically) where the probe wave will be within the PUMP strain field; these calculated locations are shown by white ellipses in Figure S.2(b,c). To estimate the cumulative strain, we integrate the strain encountered by the probe over both space (within the white ellipse) and time (the white ellipse moves as the probe moves), and then divide by the path length. This follows an established procedure Gallot et al. (2015). The results of this calculation are shown in Figure S.2(d), and demonstrate that the cumulative strain is at the frequency of the pump, and that it varies in magnitude (but not in frequency) as a function of the probe transmission delay.

References

Catheline, S., Wu, F., and Fink, M. (1999). A solution to diffraction biases in sonoelasticity: The acoustic impulse technique. *The Journal of the Acoustical Society of America*, 105(5):2941–50.
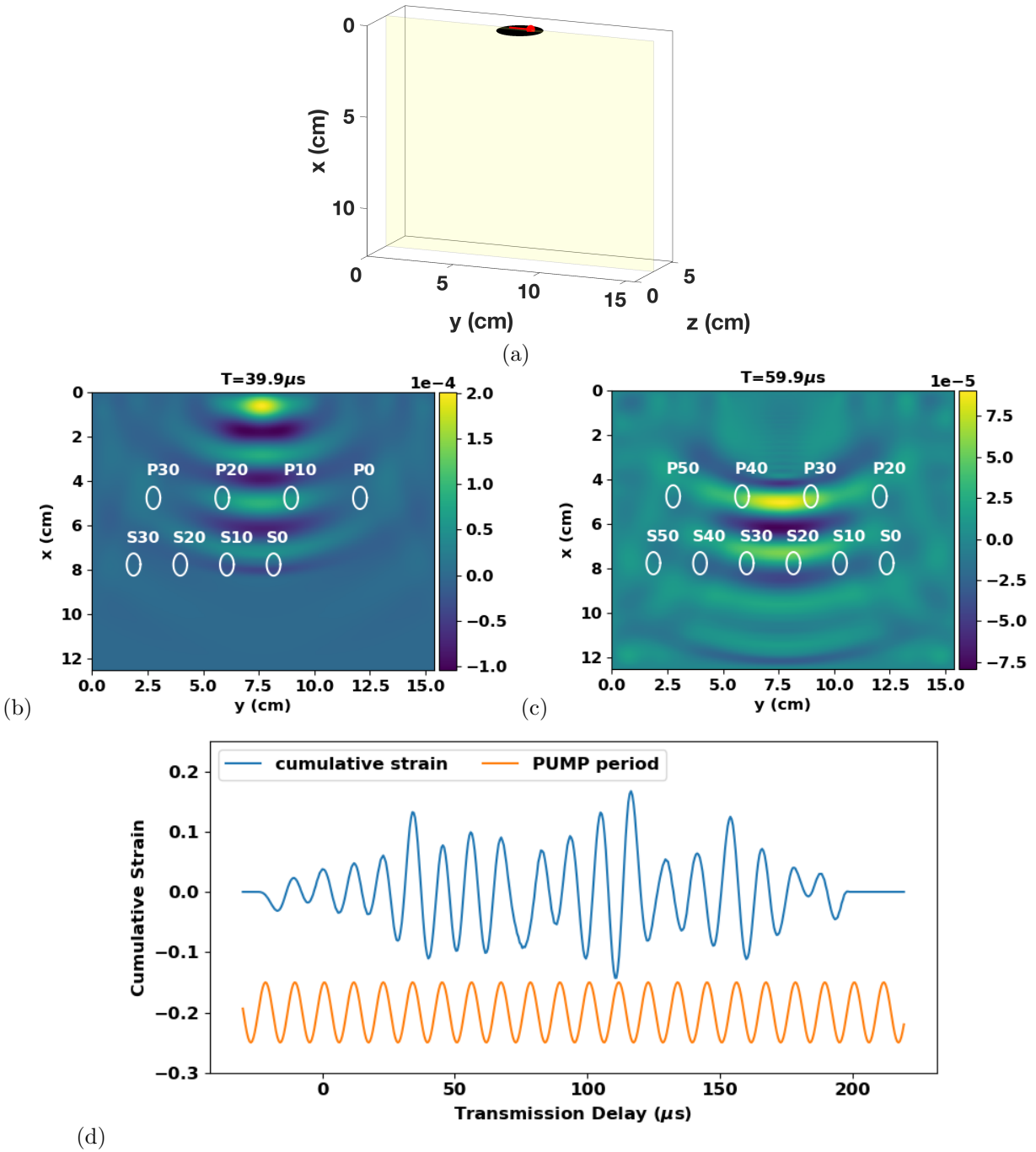
Figure S.2: (a) Schematic depiction of the numerical model. The black area in the $y - z$ plane represents the location of the pump transducer, and example snapshots are taken in the $x - y$ plane. (b,c) Example snapshots of the ϵ_{yx} component of the strain. Labels in white indicate the wave type and the transmission delay (in μs), illustrating the locations of the P- and S-probe extents for various transmission delays. (d) Modeled cumulative total strain for the P-probe, estimated by integrating the PUMP strain along the probe path for different probe transmission delays. Component breakdowns and analyses for S-probe times are given in Supplementary Figures S5 and S6, respectively.

Gallot, T., Malcolm, A. E., Szabo, T. L., Brown, S., Burns, D., and Fehler, M. (2015). Characterizing the nonlinear interaction of S- and P-waves in a rock sample. *Journal of Applied Physics*, 117:034902.

Graves, R. W. (1996). Simulating seismic wave propagation in 3d elastic media using staggered-grid finite differences. *Bulletin of the Seismological Society of America*, 86(4):1091–1106.

Khajehpour Tadavani, S., Poduska, K. M., Malcolm, A. E., and Melnikov, A. (2020). A non-linear elastic approach to study the effect of ambient humidity on sandstone. *Journal of Applied Physics*, 128(24):244902.

Renaud, G., Calle, S., Remenieras, J. P., and Defontaine, M. (2008). Exploration of trabecular bone nonlinear elasticity using time-of-flight modulation. *IEEE transactions on ultrasonics, ferroelectrics, and frequency control*, 55(7):1497–507.

Virieux, J. (1986). P-sv wave propagation in heterogeneous media; velocity-stress finite-difference method. *Geophysics*, 51(4):889–901.

Yurikov, A., Nourifard, N., Pervukhina, M., and Lebedev, M. (2019). Laboratory ultrasonic measurements: Shear transducers for compressive waves. *The Leading Edge*, 38(5):392–399.